

1 First Direct Measurements of Superheavy Element Mass Numbers

2 J. M. Gates^{1,*}, G. K. Pang¹, J. L. Pore¹, K. E. Gregorich¹, J. T. KWarsick^{1,2}, G. Savard^{3,4}, N. E. Esker⁵, M.
3 Kireeff Covo¹, M. J. Mogannam¹, J. C. Batchelder², D. L. Bleuel⁶, R. M. Clark¹, H. L. Crawford¹, P. Fallon¹,
4 K. K. Hubbard^{1,2}, A. M. Hurst², I. T. Kolaja², A. O. Macchiavelli¹, C. Morse¹, R. Orford^{3,7}, L. Phair¹, M. A.
5 Stoyer⁶

6 ¹ Lawrence Berkeley National Laboratory, Berkeley, CA 94720, USA

7 ² University of California, Berkeley, CA 94720, USA

8 ³ Argonne National Laboratory, Argonne, IL 60439, USA

9 ⁴ University of Chicago, Chicago, IL 60637, USA

10 ⁵ TRIUMF, Vancouver, BC V6T 2A3, Canada

11 ⁶ Lawrence Livermore National Laboratory, Livermore, CA 94550, USA

12 ⁷ McGill University, Montreal, QC H3A 0G4, Canada

13 PACS: 27.90.+b, 21.10.Dr, 25.70.Gh

14 * jmgates@lbl.gov

15

16 Abstract

17 An experiment was performed at Lawrence Berkeley National Laboratory's 88-Inch Cyclotron to
18 determine the mass number of a superheavy element. The measurement resulted in the observation of
19 two α -decay chains, produced via the $^{243}\text{Am}(^{48}\text{Ca},xn)^{291-x}\text{Mc}$ reaction, that were separated by mass-to-
20 charge ratio (A/q) and identified by the combined BGS+FIONA apparatus. One event occurred at $A/q=284$
21 and was assigned to ^{284}Nh ($Z=113$), the α -decay daughter of ^{288}Mc ($Z=115$), while the second occurred at
22 $A/q=288$ and was assigned to ^{288}Mc . This experiment represents the first direct measurements of the mass
23 numbers of superheavy elements, confirming previous (indirect) mass-number assignments.

24

25 Atoms of superheavy elements (SHE) have been produced at the Joint Institute for Nuclear Research (JINR)
26 in compound-nucleus reactions between ^{48}Ca projectiles and actinide targets (hot fusion reactions) for
27 nearly 20 years [1-3]. During the last several years, SHE production in such hot fusion reactions has been
28 reported from laboratories in the USA [4-6], Germany [7-11], and Japan [12], both confirming and
29 extending the JINR SHE claims. In previous discoveries up to Nh [proton number (Z) 113], mass number

30 (A) and Z assignments were made by observing the α -decay chain of a new element isotope until it
31 decayed into an isotope with well-established Z, A, and decay properties [13]. Unfortunately, all isotopes
32 of SHE produced in ^{48}Ca irradiations of actinide targets have α -decay chains that terminate with the
33 spontaneous fission of a daughter isotope, without decaying through an isotope with well-established Z
34 or A. For these SHE isotopes, presumed Z and A assignments have been made based on (i) decay
35 systematics, (ii) production rate as a function of bombarding energy (excitation functions), (iii) producing
36 the same isotopes using different target materials [cross bombardments, e.g. $^{287}\text{114}$ produced in the
37 $^{244}\text{Pu}(^{48}\text{Ca}, 5n)$ and $^{242}\text{Pu}(^{48}\text{Ca}, 3n)$ reactions] and (iv) the assumption that deexcitation of the excited
38 compound system through charged particle emission does not occur [2, 3, 13]. However, these four
39 techniques are indirect and, ultimately, depend on the accuracy of nuclear mass models [14, 15]. While it
40 is likely that the suggested Z and A assignments are correct, it is imperative that they are confirmed
41 directly through experiment. The slight, but highly consequential, possibility that the Z and A assignments
42 are systematically wrong would radically alter the interpretation and understanding of nuclear behavior
43 at the high-Z limit of stability, potentially masking unexpected and exotic nuclear phenomena.

44 In this work, we report on the first direct experimental measurements of the mass number of the SHE
45 isotopes, ^{288}Mc (Moscovium, Z=115) and ^{284}Nh (Nihonium, Z=113), produced in the $^{243}\text{Am}(^{48}\text{Ca}, 3n)^{288}\text{Mc}$
46 reaction.

47 Beams of $^{48}\text{Ca}^{11+}$ were produced from enriched-metallic Ca in VENUS (*Versatile ECR ion source for NUclear*
48 *Science*) [16, 17] and accelerated through Lawrence Berkeley National Laboratory's (LBNL) 88-Inch
49 Cyclotron to laboratory-frame energies of 262 MeV at an average intensity of 6×10^{12} ions/s for a total
50 integrated dose of 1.0×10^{18} $^{48}\text{Ca}^{11+}$ ions. The ^{48}Ca beam passed through a differential pumping section
51 separating the beamline vacuum from the 53-Pa He fill gas inside the Berkeley Gas-filled Separator (BGS)
52 [18]. Immediately downstream of the differential pumping section, the beam impinged on a rotating (~ 30
53 Hz) target wheel (radius=3.8 cm) consisting of four arc-shaped $^{243}\text{Am}_2\text{O}_3$ targets, prepared by
54 electrodeposition of ^{243}Am onto the downstream side of 2.7(1)- μm -thick Ti foils. The average ^{243}Am
55 thickness was $472 \mu\text{g}/\text{cm}^2$. Additionally, a layer of approximately $100 \mu\text{g}/\text{cm}^2$ ^{159}Tb was deposited on the
56 upstream side of the Ti foils for production of At isotopes that were used to calibrate the mass number-
57 to-charge ratio (A/q , where q is the charge state of the ion) measurements, as described below.

58 Measurement periods alternated between Mc production (8 h) and At calibration (20 min). The Mc (At)
59 ions recoiled out of (through) the targets and were separated from unreacted beam and other nuclear-

60 reaction products in the BGS, as described in previous publications [5, 18]. At the BGS focal plane the Mc
61 (At) ions passed through a 2.1- μm Ti foil and into the newly-commissioned FIONA apparatus [19]. FIONA
62 (*For the Identification Of Nuclide A*) consists of a radiofrequency (RF) gas catcher, RF quadrupole (RFQ),
63 RFQ trap, acceleration region, trochoidal spectrometer (mass analyzer), and detector station. A schematic
64 of the BGS+FIONA system is shown in Fig. 1 and the locations of the items are highlighted. Technical
65 aspects of its commissioning and operation will be described elsewhere [20]. FIONA is designed to cool
66 and bunch ions selected by the BGS before transporting them into a low-background area for A/q
67 separation and identification on a tens-of-milliseconds timescale.

68 Upon entering FIONA, the Mc (At) ions were stopped in 13 kPa of ultra-pure He inside the RF gas catcher,
69 with some retaining a positive ionic charge (see Ref [21] for a discussion of the operation of a gas catcher
70 of similar design). Then RF and DC (direct current) electric field gradients directed the ions toward the exit
71 orifice. Using a reduced ion mobility in He of $20 \times 10^{-4} \text{ m}^2/(\text{V}\cdot\text{s})$, the average drift time through the gas
72 catcher is estimated to be approximately 28 ms. After passing through the gas catcher exit orifice, the ions
73 were radially confined in the segmented RFQ, while the He gas was differentially pumped to a pressure of
74 approximately 30 Pa. An axial DC gradient, applied along the RFQ axis, directed the ions downstream
75 where they were captured in the RFQ trap, which was configured with an axial DC gradient profile to
76 create a 3-dimensional ion trap [22]. Differential pumping on this RFQ trap maintained a He pressure of
77 ~ 2 Pa in this region. Collisions with the He buffer gas in the trap region cooled the ions to several times
78 thermal energies and confined them to within $\sim 1 \text{ mm}^3$. Every 20 ms the DC voltages on the RFQ trap
79 segments were changed to eject the cooled ions into a region containing acceleration electrodes
80 (including a pulsed drift tube), steering electrodes, and Einzel lenses. The Mc^{1+} and At^{1+} ions were
81 accelerated to 3319 eV and 4789 eV, respectively.

82 After acceleration, the ions traveled through a drift region and into an area of low γ - and neutron-
83 background (separated from the BGS area by a shielding wall), where they were separated by their A/q
84 using the trochoidal spectrometer (mass analyzer) [19]. The trochoidal spectrometer consists of a
85 relatively small flat-field magnet ($l \times w \times h = 50\text{cm} \times 50\text{cm} \times 8 \text{ cm}$) with a maximum magnetic field of 1.1 T
86 in the downward (gravity) direction and perpendicular to the beam direction. Inside the magnet vacuum
87 chamber, top- and bottom-striped circuit boards with resistor chains created a uniform electric field
88 perpendicular to both the magnetic field and the velocity vector of the entering ions. By suitable choice
89 of the crossed magnetic and electric field strengths, the ions follow trochoidal trajectories [23-27]. The
90 period and beam-direction precession of these trochoids depends on the A/q and is independent of

91 velocity. Thus, A/q separation is based on the trochoid-phase difference of ions with different A/q when
92 they exit the magnetic and electric fields, which results in different exit angles in the plane defined by the
93 beam and electric field directions (dispersive plane). The FIONA A/q separation has been tested
94 extensively with ions produced at the 88-Inch Cyclotron (see below for details) and with $^{216}\text{Po}^{1+}$ ions from
95 a ^{232}U source that emanated ^{220}Rn . The trochoidal spectrometer was run using two-loop trajectories with
96 15-cm amplitudes to optimize both physical separation of adjacent masses and transportation efficiency.

97 After exiting the trochoidal spectrometer, the ions were implanted in a single-sided, 16-strip resistive
98 readout (2D-position-sensitive) detector at the FIONA focal plane, which is approximately 75 cm
99 downstream of the exit point of the trochoidal spectrometer (focal-plane detector). The focal-plane
100 detector was surrounded by a tunnel of four 16-strip single-sided silicon detectors (upstream detectors),
101 forming a combined detector array in the shape of a five-sided cube. The focal-plane detector and four
102 upstream detectors each have an active area of 58 x 58 mm and are divided into 3.625-mm wide strips.
103 Energies of events in the FIONA detector were calibrated using a source containing ^{239}Pu ($E_{\alpha}= 5156.59$
104 keV, with a branching ratio $\text{Br}_{\alpha}= 73.3\%$) ^{241}Am ($E_{\alpha}= 5485.56$ keV, $\text{Br}_{\alpha}= 84.5\%$) and ^{244}Cm ($E_{\alpha}= 5804.82$ keV,
105 $\text{Br}_{\alpha}= 76.4\%$). The positions of events in the dispersive axis of the focal-plane detector were determined by
106 resistive charge division, while the nondispersive position was given by the strip number in which that
107 event was detected. The data acquisition was triggered by either an event in the focal plane or upstream
108 silicon detectors with an energy above approximately 1 MeV.

109 In this experiment, the ion acceleration, focusing, steering and trochoidal spectrometer were calibrated
110 with $^{198-201}\text{At}^{1+}$ ions to optimize efficiency and A/q resolution. A subset of experimental data from the
111 calibration runs is shown in Fig. 2 (top, mid). At the FIONA focal plane, the A/q dispersion is approximately
112 20-mm-per-percentage difference in A/q . The mass resolving power, with separation of adjacent masses
113 at the full-width-at-tenth-maximum level, is $(A/q)/\Delta(A/q)=250$. The typical At^{1+} transport and detection
114 efficiency from the BGS focal plane, through FIONA, and to the FIONA focal-plane detector was 14(2)%
115 and was determined by comparing the measured rate of At at the BGS focal-plane detector to the
116 measured rate of At^{1+} at the FIONA focal-plane detector.

117 Scaling of FIONA from the calibration $(A/q)_{\text{calib}}$ value, obtained with At^{1+} ions, to the desired $(A/q)_{\text{new}}$ value
118 for Mc^{1+} ions was carried out by scaling the acceleration potentials such that ions corresponding to
119 $(A/q)_{\text{new}}$ have the same magnetic rigidity as those with $(A/q)_{\text{calib}}$. Therefore, no change to the trochoidal
120 spectrometer magnet was required, avoiding hysteresis effects. The voltages on the RFQ trap ejection

121 electrodes, steering and focusing electrodes, and the electrodes inside the trochoidal spectrometer were
 122 scaled by $(A/q)_{\text{calib}}/(A/q)_{\text{new}}$ to match the electric rigidity of the ions with $(A/q)_{\text{new}}$, while the time between
 123 releasing the ions from the RFQ trap and pulsing the drift tube was also scaled by $(A/q)_{\text{new}}/(A/q)_{\text{calib}}$. In this
 124 way, the Mc^{1+} ions with $(A/q)_{\text{new}}$ then take exactly the same trajectories as the calibration At^{1+} ions with
 125 $(A/q)_{\text{calib}}$. During the FIONA commissioning, the calibration procedure was tested by scaling between ions
 126 of various masses and charge states, for example $^{254}\text{No}^{2+}$, $^{255}\text{Lr}^{2+}$, $^{151}\text{Ho}^{1+}$, $^{200}\text{At}^{1+}$, $^{208}\text{Fr}^{1+}$, $^{216}\text{Po}^{1+}$, $^{245}\text{Fm}^{1+}$,
 127 $^{254}\text{No}^{1+}$ and $^{255}\text{Lr}^{1+}$. The results of these measurements are shown in Fig. 3. Based on these results, the
 128 accuracy of the A/q calibration procedure results in a ± 0.5 -mm A/q calibration error in FIONA focal-plane
 129 positions. Based on a comparison of the theoretic second ionization potential of Mc [28] to the known
 130 second ionization potentials of Fm, No, Lr, At, Po, and Fr, and the experimental ratio of $1+/2+$ ions
 131 observed at the exit of the acceleration region [Fig. 1(10)], the Mc ions are expected to retain a 1^+ charge
 132 state. Therefore, the trochoidal spectrometer was tuned such that only ions with $283 < A/q < 290$ would
 133 reach the detector during the Mc measurement runs. Given this, we do not expect to observe decays from
 134 transfer reaction products in the detector.

135 Decay chains potentially originating from Mc were identified using correlations consisting of two or more
 136 α -like events [$9 < E_{\alpha}(\text{MeV}) < 10.6$] detected within 60 s, with at least one α -like event occurring in the
 137 focal-plane detector within the same non-dispersive (y -position) range (strips 6-9) as the calibration ions.
 138 During the Mc measurement periods α -like events were observed from background from long-lived
 139 implants from previous experiments. The average rate of α -like events was 2.9×10^{-6} Hz in the focal plane
 140 and 3.9×10^{-5} Hz in the upstream detectors. During 1.7×10^5 s of running time, six of these α -like events
 141 were observed in the focal-plane detector, while eighty-one were observed in the upstream detectors.
 142 Consequently, we expect 0.03 random correlations between pairs of α -like events, with at least one α
 143 particle detected in the focal-plane detector. The expected number of random correlations between three
 144 or more unrelated α -like events is more than three orders of magnitude smaller. If one requires that the
 145 α energies closely resemble the energies along the ^{288}Mc decay chain, then the number of expected
 146 random correlations is further decreased. Given these random rates, we are confident that the events
 147 reported here are not random correlations of unrelated events.

148 The $^{243}\text{Am}(^{48}\text{Ca}, xn)$ reaction has been shown to produce three distinct α -decay chains, which have been
 149 associated with the different Mc isotopes, $A = 287, 288, 289$ [5, 11, 29]. Based on previous experiments [5]
 150 and the beam energy used in this measurement, we would expect to observe α particles originating from
 151 the presumed ^{288}Mc decay chain, which consists of five high-energy α decays with the decay properties

152 shown in Fig. 4 (left) [5, 11, 29]. The efficiency for identification of Mc decay chains in the five-sided silicon
153 detector box was modeled using Monte Carlo techniques. With an acceleration potential of 3.319 kV, the
154 Mc^{1+} implantation depth in the FIONA focal-plane detector is only ≈ 10 nm and the energy imparted into
155 the detector is below the detector threshold. Therefore, we do not record an ‘implantation’ signal and
156 the information regarding the lifetime of the first α -decay in each chain is lost. Additionally, the recoil
157 energy imparted to the α -decay daughter is sufficient to eject the daughter from the focal-plane detector
158 and into one of the upstream detectors (or to allow escape through the open end of the detector box),
159 depending on the direction of the emitted α particle. The Monte Carlo simulation modeled the position,
160 depth, and straggling of Mc ions entering the focal-plane detector. For each α -decaying chain member,
161 the isotropic emission of α particles with known energy and the recoil of the α -decay daughter were
162 modeled. If detection of at least two (three) of the five α decay chain members is required for ^{288}Mc
163 identification the efficiency is 93% (85%). The Monte Carlo simulation was also repeated for the four-
164 member ^{284}Nh decay chains (under the scenario that the α decay of the parent ^{288}Mc occurred in the gas
165 catcher), resulting in an efficiency of 88% (69%) for detecting at least two (three) of the four α -decay chain
166 members. The simulations also show that the position of the first α decay detected in the focal-plane
167 detector is always the implantation site of the initial ion.

168 Two decay chains were observed as shown in Fig. 4 (right). The first decay chain consisted of an α particle
169 with $E_{\alpha}=9.93(6)$ MeV followed 34.376 s later by an α particle with $E_{\alpha}=9.19(6)$ MeV. The energy of the first
170 observed α particle is consistent with the energy of the α decay that is typically assigned to ^{284}Nh ($E_{\alpha}=9.98$
171 MeV, $t_{1/2}=0.94$ s), while the energy and lifetime of the second α particle corresponds to the known decay
172 properties of the presumed ^{272}Bh ($E_{\alpha}=9.08$ MeV, $t_{1/2}=11.0$ s). This decay chain was detected at a dispersive
173 (x -) position of 22.4 mm, near the expected peak of the $A/q=284$ distribution ($x=23.2$ mm), as shown in
174 Fig. 2 (bottom). Given that we estimate the residence time in the gas catcher to be approximately 28 ms
175 (see earlier discussion), while the half-life of ^{288}Mc is approximately 160 ms, we expect at least 10% of the
176 Mc events to α decay inside the gas catcher. There are also other processes which can increase the Nh/Mc
177 ratio exiting the gas catcher, such as a neutral Mc α decaying to produce a charged Nh. The observed α -
178 particle energies, lifetimes, and position are then all consistent with the interpretation of this event as
179 arising from a ^{288}Mc ion α decaying inside the gas catcher to the detected ^{284}Nh .

180 A second observed decay chain consisted of four α particles, detected within 20 s, and is also shown in
181 Fig. 4 (right). The energies and lifetimes of the observed α particles are consistent with the properties

182 currently assigned to the isotopes ^{288}Mc , ^{280}Rg , ^{276}Mt and ^{272}Bh . The first three α particles were observed
183 in the upstream detectors, with the fourth α particle observed in the focal-plane detector at a position of
184 51.9 mm, near the peak of the expected $A/q=288$ mass distribution ($x=51.2$ mm), as shown in Fig. 2
185 (bottom).

186 Assuming (i) a ^{288}Mc production cross-section of 8.5 pb [29], (ii) the Mc^{1+} transmission efficiency is the
187 same as the At^{1+} transmission efficiency and (iii) the ^{243}Am targets were not damaged during irradiation,
188 then we would have expected 5.2 events and saw 2. The probability of seeing two or less events when
189 you expect 5.2 is 11%.

190 To determine the likelihood that these decay chains originated from ^{288}Mc (and its daughter ^{284}Nh) as
191 opposed to neighboring isotopes, A/q calibrations with $^{198-201}\text{At}$ were measured before and after the Mc
192 and Nh events to determine the A/q peak centroids, Lorentzian peak width, and A/q dispersion. These
193 parameters were then used to predict the peak shapes and positions for SHE ions. The probabilities that
194 the two-member event chain (first event) corresponds to the implantation of an ion with $A/q=285$, 284,
195 or 283 are 13%, 81%, and 7%, respectively. For the four-member event chain (second event) the
196 probabilities for $A/q=289$, 288, or 287 are 10%, 83% and 7%, respectively. Previous studies [5, 11, 29] have
197 shown that decay chains originating from this target-projectile combination can be sorted into three
198 groups, each with distinct decay properties [29, 30]. Both events presented in this work have α -particle
199 energies and lifetimes that are associated with the decay chains that have been previously assigned to
200 ^{288}Mc – which proceed through the five-member α -decay chain shown in Fig. 4 (left). Accordingly, we have
201 assumed that these two event chains originate from the same isotope, that which has been assigned to
202 ^{288}Mc . Applying the constraint that the detected focal plane positions differ by four A/q units, the
203 combined implantation assignment as $A/q=288$ and 284 has a confidence level of 97.6%. Accordingly, we
204 assign these two event chains to the production and decay of ^{288}Mc .

205 To assess the effect of uncertainties on our A/q assignment confidence level, a Monte Carlo Maximum
206 Likelihood calculation was carried out. Uncertainties in the At peak centroids, Lorentzian peak widths, and
207 the A/q dispersion were determined from fits to the experimental At A/q spectrum shown in Fig. 2
208 (middle). For each of the 10^4 Monte Carlo trials, the ^{200}At centroid, peak width, and dispersion were
209 sampled from the normal distributions determined from the fits. With the constraint that the A/q of the
210 first member of the 4- α event chain is four units larger than the first member of the 2- α chain, the
211 ensemble of properly normalized likelihood probabilities for the $A/q=288$ and 284 assignments has a

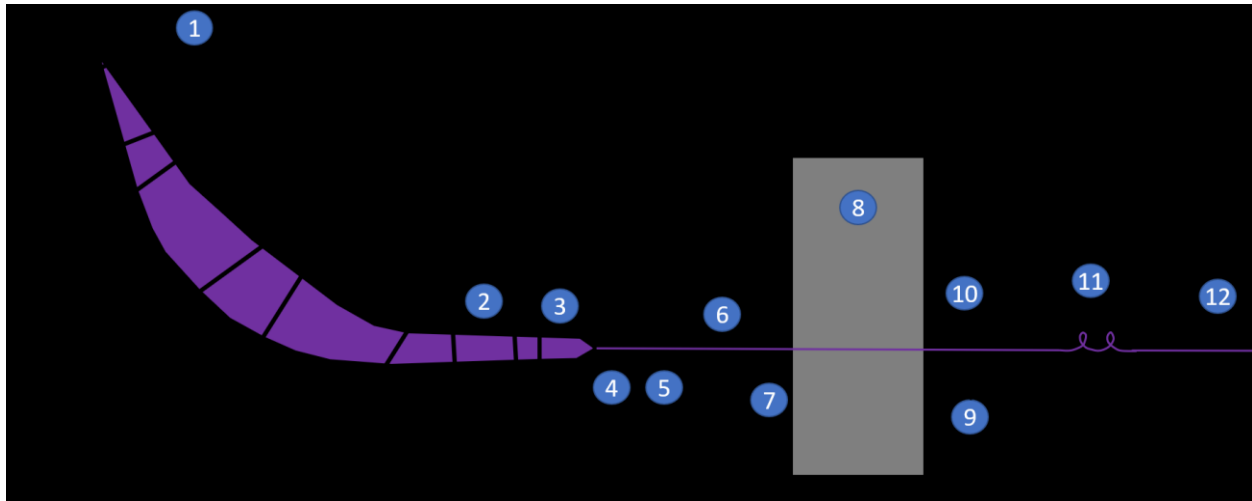
212 narrow distribution with a median likelihood of 97.2%. This shows that the uncertainties have little effect
213 on the A/q assignment confidence level.

214 In this Letter, we have reported the first experimental determination of the mass numbers of superheavy
215 element isotopes. With few exceptions [30], the data obtained from excitation functions, decay
216 systematic and cross bombardments indicate that the SHE assignments form a contiguous group in Z and
217 A , with correct *relative* mass numbers. If one accepts this premise, our direct experimental measurement
218 of the mass numbers of ^{288}Mc and ^{284}Nh anchor most of the previously reported SHE A assignments, thus
219 finally confirming that most of the mass numbers suggested for other superheavy element isotopes are
220 correct.

221 **Acknowledgements**

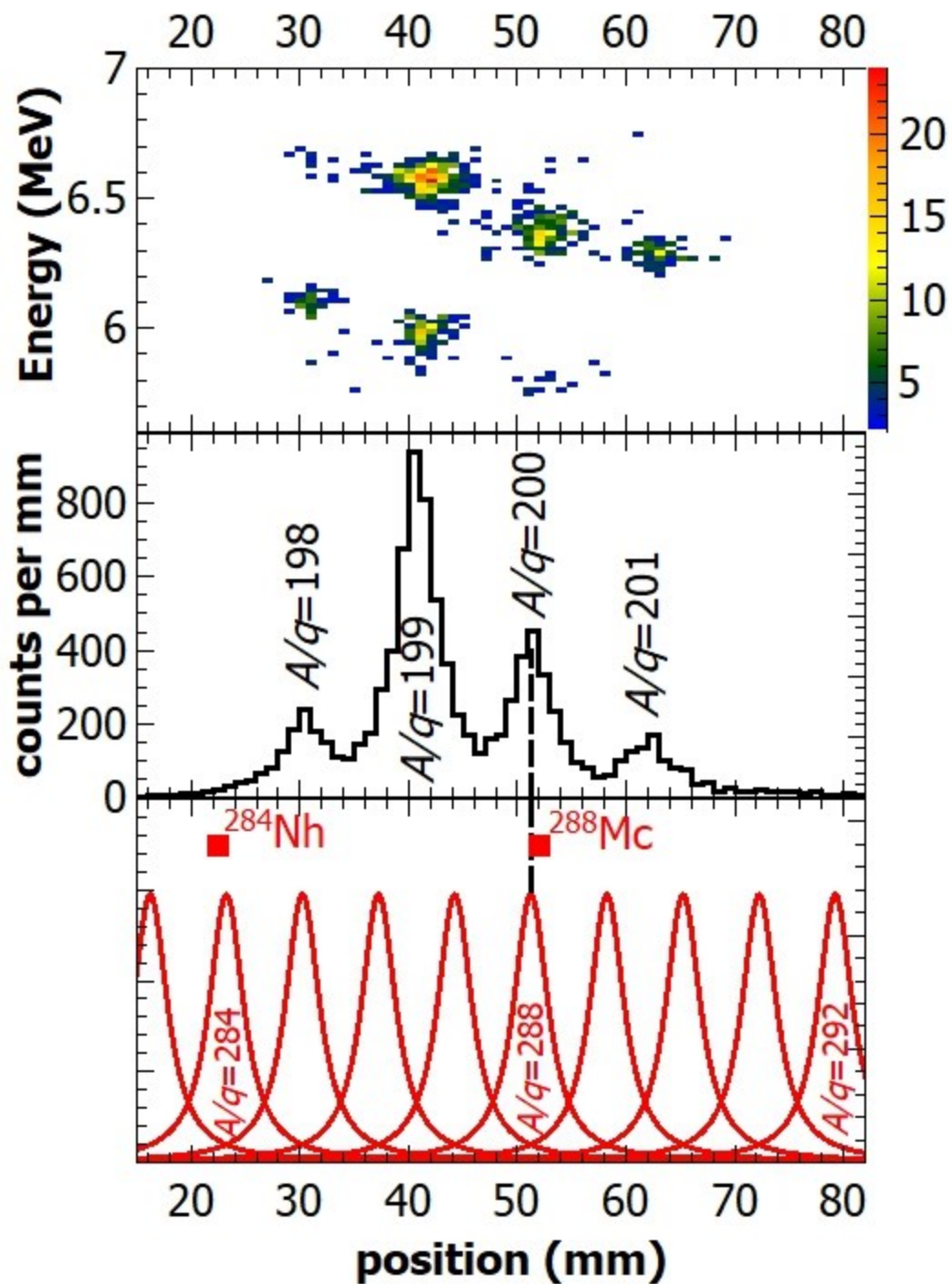
222 We gratefully acknowledge the operations staff of the 88-Inch Cyclotron for providing the intense beams
223 of ^{48}Ca and stable operating condition. We would also like to acknowledge all the help we received from
224 the Cyclotron technical and engineering staff during the construction of FIONA. This work was supported
225 in part by the U.S. Department of Energy, Office of Science, Office of Nuclear Physics under contract
226 numbers DE-AC02-05CH11231 (LBNL), DE-AC02-06CH11357 (ANL) and DE-AC52-07NA27344 (LLNL). The
227 authors are indebted (for the use of ^{243}Am) to the Division of Chemical Sciences, Office of Basic Energy
228 Services, U.S. Department of Energy, through the transplutonium element production facilities at Oak
229 Ridge National Laboratory. JMG is the recipient of a U.S. Department of Energy, Office of Science, Early
230 Career Award.

231



232

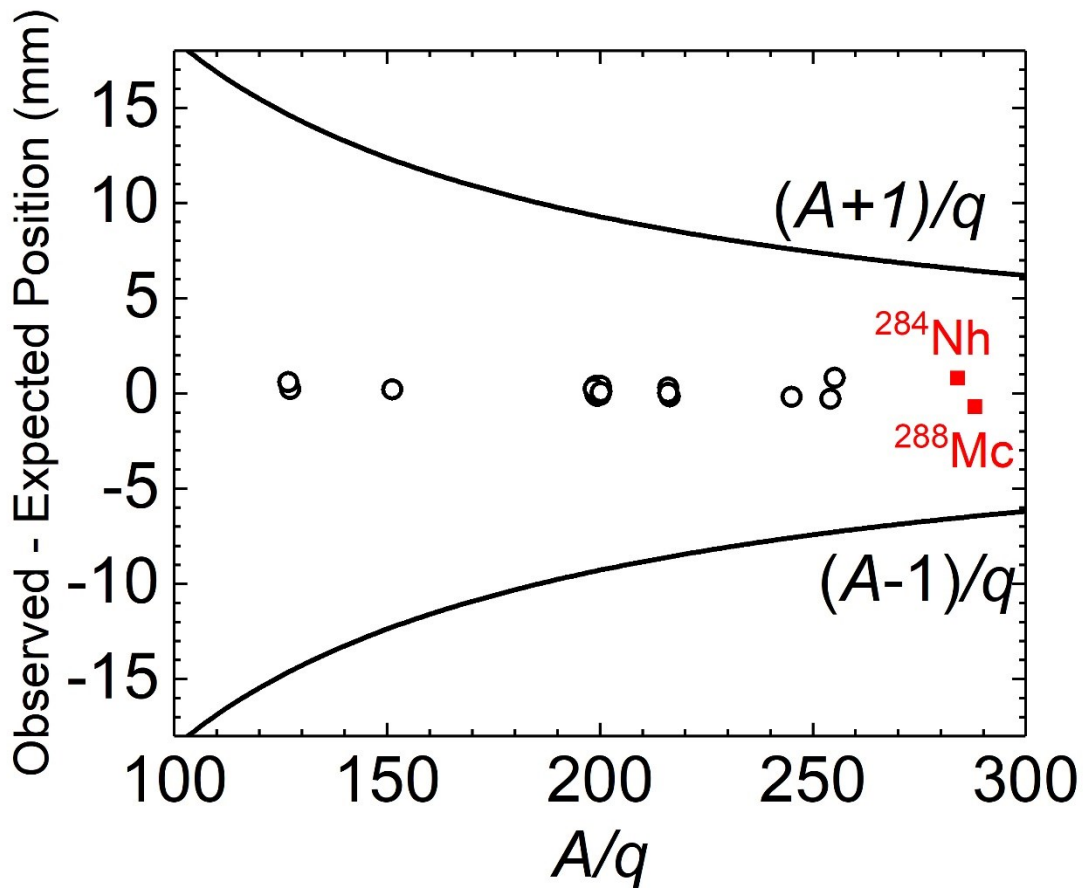
233 FIG. 1: Schematic of BGS+FIONA with the labels indicating the positions of (1) BGS (2) BGS focal plane
 234 detector (3) Gas catcher (4) RFQ (5) RFQ trap (6) acceleration region (7) focusing element, horizontal and
 235 vertical steerers (8) shielding wall (9) focusing element, horizontal and vertical steerers (10) C2 detector
 236 (11) trochoid spectrometer (12) FIONA focal-plane detector. The purple shaded area/line represent the
 237 beam image of ^{288}Mc traveling through the BGS and FIONA.



238

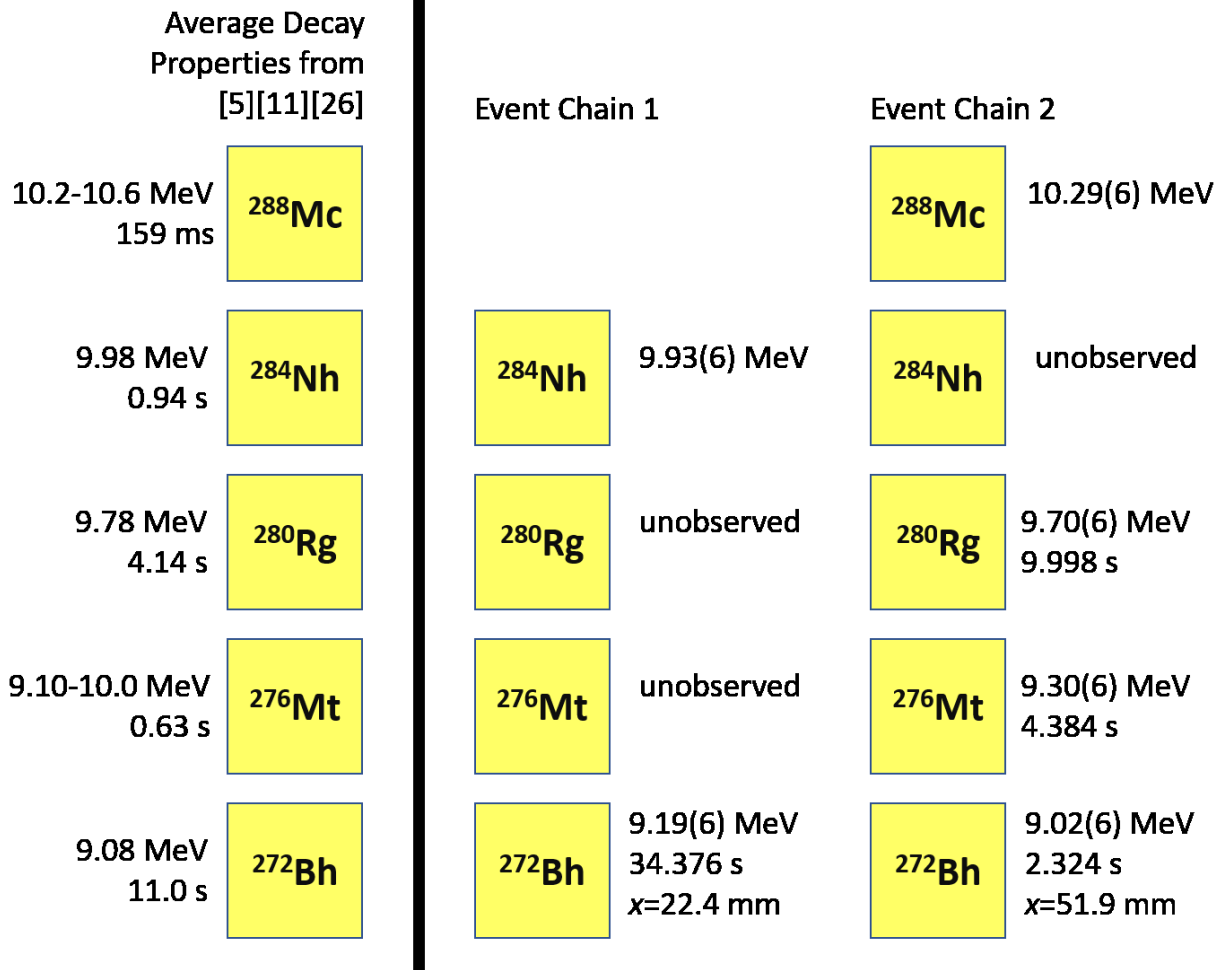
239 FIG. 2: (top) Experimental data from the At^{1+} calibration run showing the α -particle energies versus the
 240 positions they were observed in the focal plane detector; (middle) Experimental data from the At^{1+}
 241 calibration runs taken before and after each event was observed and showing the A/q separation;

242 (bottom) Expected location of $A/q=283-292$ mass peaks at the FIONA focal-plane detector. The locations
 243 of the two observed events are shown by the squares.



244
 245 FIG. 3: Deviation of the observed focal plane position from the expected position (after scaling) as a
 246 function of A/q . The open circles correspond to the results for known isotopes, $^{254}\text{No}^{2+}$, $^{255}\text{Lr}^{2+}$, $^{151}\text{Ho}^{1+}$,
 247 $^{200}\text{At}^{1+}$, $^{208}\text{Fr}^{1+}$, $^{216}\text{Po}^{1+}$, $^{245}\text{Fm}^{1+}$, $^{254}\text{No}^{1+}$ and $^{255}\text{Lr}^{1+}$ and the error bars are smaller than the symbols. The red
 248 squares correspond to the two events of ^{284}Nh and ^{288}Mc discussed in the text. The lines represent the
 249 expected centroids of masses with $(A\pm 1)/q$ from the scaled mass. From the commissioning measurements,
 250 the observed position agrees within ± 0.5 mm of the predicted (scaled) position, giving a position
 251 uncertainty that is small compared to the separation between adjacent mass numbers.

252



253

254 FIG. 4: (left) Average of known decay properties assigned to ^{288}Mc and its daughters [5, 11, 29]; (right)
 255 Details of decay chains detected at the FIONA focal plane. Unobserved decays within each decay chain
 256 are indicated as “unobserved” and are assumed to have been emitted out of the open end of the detector
 257 array. The x-position of decays observed in the focal-plane detector is also given.

258

- 259 [1] Yu. Ts. Oganessian, J. Phys. G **34**, R165 (2007).
 260 [2] Yu. Ts. Oganessian and V. K. Utyonkov, Rep. Prog. Phys. **78**, 036301 (2015).
 261 [3] Yu. Ts. Oganessian and V. K. Utyonkov, Nucl. Phys. A **944**, 62 (2015).
 262 [10.1016/j.nuclphysa.2015.07.003](https://doi.org/10.1016/j.nuclphysa.2015.07.003)
 263 [4] P. A. Ellison *et al.*, Phys. Rev. Lett. **105**, 182701 (2010).
 264 [5] J. M. Gates *et al.*, Phys. Rev. C **92**, 021301 (2015).
 265 [6] L. Stavsetra, K. E. Gregorich, J. Dvorak, P. A. Ellison, I. Dragojevic, M. A. Garcia and H. Nitsche, Phys.
 266 Rev. Lett. **103**, 132502 (2009).
 267 [7] Ch. E. Düllmann *et al.*, Phys. Rev. Lett. **104**, 252701 (2010).

- 268 [8] S. Hofmann *et al.*, Eur. Phys. J. A **32**, 251 (2007).
269 [9] S. Hofmann *et al.*, Eur. Phys. J. A **48**, 62 (2012).
270 [10] J. Khuyagbaatar *et al.*, Phys. Rev. Lett. **112**, 172501 (2014).
271 [11] D. Rudolph *et al.*, Phys. Rev. Lett. **111**, 112502 (2013).
272 [12] D. Kaji *et al.*, J. Phys. Soc. Japan **86**, 034201 (2017). 10.7566/JPSJ.86.034201
273 [13] K. Gregorich, EPJ Web Conf. **131**, 06002 (2016).
274 [14] G. Audi, M. Wang, A. H. Wapstra, F. G. Kondev, M. MacCormick, X. Xu and B. Pfeiffer, Chinese Phys.
275 C **36**, 1287 (2012).
276 [15] M. Wang, G. Audi, A. H. Wapstra, F. G. Kondev, M. MacCormick, X. Xu and B. Pfeiffer, Chinese Phys.
277 C **36**, 1603 (2012).
278 [16] D. Leitner, C. M. Lyneis, T. Loew, D. S. Todd, S. Virostek and O. Tarvainen, Rev. Sci. Instrum. **77**,
279 03A302 (2006).
280 [17] C. M. Lyneis, D. Leitner, M. Leitner, C. Taylor and S. Abbot, Rev. Sci. Instrum. **81**, 02A201 (2010).
281 10.1063/1.3271135
282 [18] K. E. Gregorich, Nucl. Instrum. Methods A **711**, 47 (2013). [10.1016/j.nima.2013.01.020](https://doi.org/10.1016/j.nima.2013.01.020)
283 [19] J. M. Gates, EPJ Web Conf. **131**, 08003 (2016).
284 [20] J. M. Gates, K. E. Gregorich, N. E. Esker, G. K. Pang, J. L. Pore, J. T. Kwarsick and G. Savard, (to be
285 published).
286 [21] G. Savard, J Phys. **312**, 052004 (2011). doi:10.1088/1742-6596/312/5/052004
287 [22] F. Herfurth *et al.*, arXiv arXiv:nucl (2000). <https://arxiv.org/abs/nucl-ex/0011021v1>
288 [23] T. Mariner and W. Bleakney, Rev. Sci. Instrum. **20**, 297 (1949).
289 [24] G. W. Monk and G. K. Werner, Rev. Sci. Instrum. **20**, 93 (1949).
290 [25] C. F. Robinson and L. G. Hall, Rev. Sci. Instrum. **27**, 504 (1956).
291 [26] K. Yano and S. H. Be, Jpn. J. Appl. Phys. **19**, 1019 (1980).
292 [27] W. Bleakney and J. A. Hipple, Phys. Rev. **53**, 521 (1938).
293 [28] A. Borschevsky, L. F. Pasteka, V. Pershina, E. Eliav and U. Kaldor, Phys. Rev. A **91**, 020501(R) (2015).
294 [29] Yu. Ts. Oganessian *et al.*, Phys. Rev. C **87**, 014302 (2013).
295 [30] U. Forsberg *et al.*, Nucl. Phys. A **953**, 117 (2016). [10.1016/j.nuclphysa.2016.04.025](https://doi.org/10.1016/j.nuclphysa.2016.04.025)

296